Nisula, Mikko; Karppinen, Maarit

Atomic/Molecular Layer Deposition of Lithium Terephthalate Thin Films as High Rate Capability Li-Ion Battery Anodes

Published in:
Nano Letters

DOI:
10.1021/acs.nanolett.5b04604

Published: 01/01/2016

Document Version
Peer reviewed version

Please cite the original version:
Nisula, M., & Karppinen, M. (2016). Atomic/Molecular Layer Deposition of Lithium Terephthalate Thin Films as High Rate Capability Li-Ion Battery Anodes. *Nano Letters*, *16*(2), 1276-1281.
https://doi.org/10.1021/acs.nanolett.5b04604

Atomic/molecular layer deposition of lithium terephthalate thin films as high rate capability Li-ion battery anodes

Mikko Nisula and Maarit Karppinen*

Department of Chemistry, Aalto University, P.O. Box 16100, FI-00076 Espoo, Finland

Keywords: Atomic layer deposition, molecular layer deposition, thin film battery, organic electrode

ABSTRACT: We demonstrate the fabrication of high-quality electrochemically active organic lithium electrode thin films by the currently strongly emerging combined atomic/molecular layer deposition (ALD/MLD) technique using lithium terephthalate, a recently found anode material for lithium-ion battery (LIB), as a proof-of-the-concept material. Our deposition process for Li-terephthalate is shown to well comply with the basic principles of ALD-type growth including the sequential self-saturated surface reactions, a necessity when aiming at micro-LIB devices with 3D architectures. The as-deposited films are found crystalline across the deposition temperature range of 200 – 280 °C, which is a trait highly desired for an electrode material but rather unusual for hybrid organic-inorganic thin films. Excellent rate capability is ascertained for the Li-terephthalate films with no conductive additives required. The electrode performance can be further enhanced

by depositing a thin protective LiPON solid-state electrolyte layer on top of Li-terephthalate; this yields highly stable structures with capacity retention of over 97 % after 200 charge/discharge cycles at 3.2 C.

The miniaturization of electronic devices demands for energy storage systems of equal dimensions. In order to retain reasonable energy and power densities, all-solid-state thin-film microbatteries based on three-dimensional (3D) microstructured architectures are seen as a viable solution. Compared to 2D thin-film batteries, the increased specific surface area of 3D microstructures provides us with enhanced energy density while the electrodes can still be kept thin enough for short Li diffusion paths and thereby good power density.[1–3] Such an approach places an apparent need for a thin-film deposition method capable of manufacturing the electrode and electrolyte materials on high-aspect-ratio substrates. Atomic layer deposition (ALD) is an established thin-film technology for producing conformal coatings on such high-aspect-ratio structures.[4,5] It is based on sequential exposure of gaseous precursors on the target substrate where surface-saturation limited reactions allow the layer-by-layer deposition of high-quality thin films with sub-monolayer accuracy.[6] However there is an apparent need for broadening the currently rather narrow range of available deposition processes for Li-ion electrode materials.

Organic electrode materials would possess several attractive features compared to the current transition-metal based inorganic materials. They are composed of cheap, earth-abundant, environmentally friendly and light elements, and owing to the low molecular mass together with a possibility for multiple redox processes per molecule, organic electrodes display very high theoretical specific capacities of several hundred mAh per gram. Moreover, the redox properties can be tuned by the addition of electron donating/withdrawing functional groups. The biggest

obstacles in putting organic electrode materials into practical use in next-generation LIBs are their instability/dissolution in the commonly employed liquid electrolytes and their negligible electronic conductivity which dictates the need for very large amounts of conductive additives resulting in greatly reduced actual capacities.[7,8] In an all-solid-state thin-film LIB these obstacles could possibly be circumvented: the dissolution issue would be completely avoided by replacing the liquid electrolyte by a solid one, while the reduced dimensions in thin films should contribute towards mitigating the effect of intrinsically poor electronic conductivity of organics.

Owing to the recent progress in combining the ALD technique for inorganic materials with the strongly emerging molecular layer deposition (MLD) technique for organics it has become possible to fabricate inorganic-organic hybrid thin films in a well-controlled atomic/molecular layer-by-layer manner; for a recent review of the combined ALD/MLD technique see ref. 9. A number of ALD/MLD processes with different organic constituents have already been developed. However, the range of the metal components is yet limited, and as far as we know no ALD/MLD processes for lithium-organic thin films have been reported. Here we demonstrate that the ALD/MLD technique indeed is commendably suited for the deposition of organic LIB electrodes; our proof-of-the-concept data are for lithium terephthalate ($Li_2C_8H_4O_4$ or LiTP). The electrochemical activity of bulk LiTP was discovered by Tarascon *et al.*;[10] their data revealed high gravimetric capacity of 300 mAh/g associated with a flat reduction potential at around 0.8 V vs. Li^+/Li. As such LiTP is indeed an attractive anode material as it offers considerably higher specific energy compared to other electrode material candidates for thin-film LIBs including TiO_2 and $Li_4Ti_5O_{12}$.[2] Moreover, computational predictions indicate that the volume change of LiTP during (de)lithiation is relatively small, i.e. ~6 %.[11] Hence LiTP would be preferable also over the traditional high-capacity anode materials such as silicon and transition-metal oxides for which the

large volume expansion during lithiation results in poor cycle life of the material.[12] The major findings of the present study are three-fold. First, we succeeded in fabricating crystalline organic LIB electrode thin films for the first time through a gas-phase deposition technique. Secondly, the films were found to be electrochemically active with excellent rate capability without relying on any conductive additives thus demonstrating that LiTP can perform as a high-rate anode material if the electronic conductivity issue can be overcome. Lastly we show that by applying a protective layer consisting of the lithium phosphorus oxynitride (LiPON) solid-state electrolyte deposited by ALD, the LiTP electrodes can be stabilized even in $LiPF_6$-based liquid electrolytes resulting in an excellent cycle life.

The LiTP thin films were deposited using Li(thd) (thd = 2,2,6,6-tetramethyl-3,5-heptanedionate) and terephthalic acid (TPA) as precursors. The defining feature of an ALD/MLD process is the self-limiting film growth, that is, after a certain threshold value, the growth-per-cycle (GPC) calculated from the resultant film thickness value (determined in our case by spectroscopic ellipsometry) becomes constant regardless the pulsing times of the precursors. To verify the ALD/MLD-type film growth, the deposition rate for our Li(thd)–TPA process was studied as a function of the precursor pulse lengths at a deposition temperature of 200 °C using 200 ALD/MLD cycles. As shown in Figure 1a, in the case of Li(thd), saturation is achieved with a pulse length of 4 s whereas TPA requires a longer pulse length of 10 s. With these optimized pulse lengths the saturation-limited growth rate at 200 °C is ~3.0 Å/cycle. The saturation limited growth was further investigated by depositing LiTP thin films on microstructured silicon substrates consisting of trenches ~50 µm deep and 7.5 µm wide using the aforementioned pulse and purge lengths with 400 deposition cycles. As shown in Figure S1 in Supporting Information, essentially conformal films are achieved even with parameters optimized for planar substrates.

Using the same pulse lengths, the growth rate was further studied in a temperature range of 200 – 280 °C using 400 ALD/MLD cycles. From Figure 1b, no region of constant GPC value, i.e. a so-called ALD window, is observed; instead there is a rather monotonous decrease in GPC with increasing deposition temperature which is actually a common feature for a majority of ALD/MLD processes.[9,13,14] The density of the films, as obtained from the X-ray reflectivity (XRR) data, appears to remain essentially constant in the deposition temperature range of 200 – 240 °C (Figure 1b**)**. At temperatures higher than this, the decrease in density might arise from thermal decomposition of either of the precursors resulting in inclusion of carbon impurities. Within the uniform density region, the resultant film density of ~1.4 g/cm^3 is in a rather good agreement with the ideal density of bulk LiTP (1.6 g/cm^3) calculated from its crystal structure proposed in ref. 18. As shown in Figure 1c, instead of the expected linear relationship between the film thickness and the number of deposition cycles, the growth rate increases with increasing number of deposition cycles. The growth rate nears constant after 200 deposition cycles. Simultaneously, an opposite trend is seen in the film density which decreases until reaching a stable value of 1.4 g/cm^3 after 200 deposition cycles. The film thicknesses up to 100 deposition cycles were crosschecked using X-ray reflectivity (XRR) measurements (Table S1). As the roughness of the samples prevented the use of XRR on the thicker samples, the thickness of the sample with 400 deposition cycles was measured also from a scanning electron microscopy (SEM) cross-section image.

Atomic force microscopy (AFM) image taken after 70 deposition cycles (Figure 2a) shows distinct granular shapes with voids in between. The average feature height of 20 nm matches well with the film thickness obtained with ellipsometry. In the AFM image taken after 400 deposition cycles (Figure 2b) the granular features have gained in size and coalesced forming a more continuous film. In between the granules there appear to be deep voids and the overall roughness

of the sample is quite high. As such, the nonlinearity of could possibly be explained by the island growth model of crystalline films.[15,16] The initial nucleation and growth is not uniform; instead, distinct islands are formed, which grow in size as the deposition proceeds. A constant-growth regime is achieved only after the islands have coalesced and formed a continuous layer. As the growth rate along different lattice planes varies, during the coalescence parts of the film can become inaccessible forming voids within the films thus explaining the decrease in the apparent density.

Grazing incidence X-ray diffraction (GIXRD) data do indeed confirm that the as-deposited films are highly crystalline at all deposition temperatures which is unusual for ALD/MLD inorganic-organic hybrid thin films.[9] To our best knowledge, thus far only one report exists on crystalline ALD/MLD thin films.[17] The GIXRD patterns could be indexed in space group $P2_1/c$ according to the crystal structure proposed by Kaduk[18] for LiTP with no additional reflections (Figure 2c). The lattice parameters were determined to be, a = 8.36 Å, b = 5.12 Å, c = 8.46 Å, β = 93.08 °, in an excellent agreement with those reported for bulk LiTP.[10,18] The FWHM value of the 011 peak (Figure S2a and S2b) decreases with increasing number of deposition cycles indicating an increase in the crystallite size. Such an observation is in line with the proposed island-type growth mode. As with the GPC and density values, the FWHM values appear to level off after 200 deposition cycles. Additional X-ray diffraction measurements conducted in the Bragg-Brentano configuration revealed only the most prominent 110 and 102 peaks indicating that the films are polycrystalline without any evident orientation effect.

Fourier transform infrared spectroscopy (FTIR) studies were carried out to further elucidate the structure of our LiTP thin films. In the FTIR spectrum (Figure 2d) the dominant absorption peaks at 1392 and 1570 cm^{-1} arise from the symmetric and asymmetric stretching of the carboxylate

group, respectively. The values are in good agreement with those reported for bulk LiTP.[10,19] The peak separation, i.e. 178 cm^{-1}, indicates towards a structure where Li is in a bridging position,[20,21] in accordance with the crystal structure proposed for LiTP. Additionally, at ~523 cm^{-1} a characteristic peak of Li-O bond can be observed. The lack of characteristic absorption bands due to -OH stretching in the region of 2500 - 3000 cm^{-1} indicates that during the deposition process TPA has fully reacted as intended with no inclusions of the unreacted precursor in the films.[22] Also no traces of Li_2CO_3 and LiOH were detected and no changes were seen in the FTIR spectrum even after extended storage (6 months) of the films in ambient atmosphere (Figure S3). The surface composition for a fresh and aged sample were probed with X-ray photoelectron spectroscopy (XPS). As shown in Figure S4, the long storage time has not resulted in significant changes in the spectrum. While the similarities of the chemical environments of carbonate and carboxylate group make the analysis somewhat ambiguous, we conclude that Li_2CO_3 is not formed on the films surface based on the following observations. For lithium carbonate, the CO_3^{2-} signal should be seen at 290 eV. Instead, a peak at 289.0 eV is detected, which matches with values reported for the carboxylate group.[23] Furthermore, the Li 1s peak is detected at 55.8 eV, while for Li_2CO_3 the peak should be located at 55.2 - 55.4 eV. While the shift is relatively minor, it is in the opposite direction as compared to the carboxylate/carbonate peak thus ruling out a systematic error in the measurements. Lastly, the ratio of oxygen vs. carboxylate-type carbon is 1.9:1, which matches quite well with the expected ratio of 2:1

The electrochemical performance of the LiTP films was evaluated using conventional $LiPF_6$ based liquid electrolyte coin cells in order to establish that the electrochemical characteristics match those previously reported[10] for bulk LiTP electrodes. LiTP deposited on a stainless steel substrate was employed as the working electrode and Li foil as the counter electrode. In order to

158 shield the electrodes from the liquid electrolyte and to mimic the situation in all-solid-state LIBs
159 regarding the electrode-solid electrolyte interface, samples with 600 ALD cycles of LiPON solid
160 electrolyte layer on the surface were manufactured using our recently developed ALD process for
161 LiPON.[24] Assuming a growth rate of ~0.7 Å/cycle, this would add up to a layer of ~40 nm. Figures
162 3a and 3b display the cyclic voltammograms recorded for the bare and LiPON-coated LiTP films,
163 respectively. The as-deposited films are indeed electrochemically active but for the bare LiTP film
164 the initial cycle differs greatly from the following ones with a broad reduction peak appearing at
165 around 0.4 V. For the subsequent two cycles, a much sharper peak at 0.76 V is observed but the
166 peak current density decreases from 52 to 42 $\mu A/cm^2$ between the second and third cycle. The
167 anodic sweep is identical for each cycle with three oxidation peaks appearing at 0.89, 1.00, and
168 1.06 V. For the LiTP-LiPON case, the initial wide reduction peak is not seen, but instead a sharp
169 reduction peak with a constant peak current density of 40 $\mu A/cm^2$ appears at 0.79 V during each
170 cycle. Also, the anodic peak at 1.06 V is not existing and the one at 0.89 is significantly reduced.
171 Thus the data seem to implicate that a solid electrolyte interface (SEI) layer is formed on the bare
172 LiTP anode either directly due to immersion in the liquid electrolyte or during the initial cathodic
173 scan. Furthermore, during subsequent CV measurements at varying scan rates (data not shown
174 here), the initial broad reduction peak was always observed after the cell had been left to stabilize
175 in between the scans. The LiPON layer however was found to stabilize the LiTP-anode without
176 reducing the peak currents, i.e. not increasing the cell resistance, and the reduction peaks remained
177 sharp and consistent also with the higher scan rates.

178 Similar behavior was observed also in the initial charge/discharge conducted at a voltage range
179 of 0.4 - 3.0 V vs Li^+/Li with a current rate of 0.5 $\mu A/cm^2$ (Figure 3c). During the initial discharging
180 a distinct plateau at 0.8 V is observed for both the bare and the LiPON-coated LiTP electrodes

with the latter one demonstrating a slightly lower polarization consistent with the CV data. However the amount of irreversible capacity is much higher with the bare LiTP film resulting in an initial coulombic efficiency of 0.50 while the LiPON coating increases the efficiency to 0.64. The larger irreversible capacity of the bare LiTP also implies formation of a SEI layer during the cycling.

The electrochemical performance was further tested by cycling the electrodes at various current rates at a voltage range of 0.4 - 3.0 V vs Li^+/Li. Because the mass of the electrodes could not be reliably assessed, here the C-rates are calculated assuming the reversible capacity obtained from the initial charge/discharge conducted at a very low current rate of 0.5 $\mu A/cm^2$ to be equal of the full capacity. Assuming an electrode thickness of 170 nm and density of 1.4 g/cm^3 as obtained from ellipsometry and XRR measurements, respectively, for a comparable sample deposited on silicon, the measured reversible capacity would correspond to a specific capacity of approximately 350 mAh/g. As we were unable to measure the thickness directly from the stainless steel substrate, the value is only directional due to possible differences in the growth rate. While higher than the theoretical capacity assuming two electron transfer reactions per molecule, it is not unreasonable as recently Lee *et al.*[25] revealed that LiTP may undergo further lithium insertions when cycled below 0.7 V vs Li^+/Li bringing the actual specific capacity up to 522 mAh/g when discharged to 0.0 V vs. Li/Li^+. As shown in Figure 4a, both LiTP and LiTP-LiPON perform very well up to 6.4 C retaining approximately 69 and 66 % of the initial capacity, respectively at that current rate. At higher current rates, the bare LiTP electrode fails completely while the LiPON-coated LiTP electrode retains a very respectable performance delivering over 50 % of the initial capacity at ~20 C, i.e. charge/discharge in 3 min, and even at 64 C, i.e. charge/discharge in 56 s, the electrode still retains 23 % of the full capacity. The high rate performance is not unexpected as according to

density functional theory calculations conducted by Zhang et al.[11], the rate capability of LiTP should inherently be excellent due to the low activation energy of lithium diffusion. Thus it is apparent that the limited performance of bulk LiTP is indeed due to the poor electronic conductivity, and this can be circumvented with the reduced dimensions of our thin-film electrodes without relying on conductive additives. The reason for the sudden failure of the bare LiTP is evident from the voltage curves recorded at increasing current rates shown in Figures 4b and 4c. The bare LiTP electrode displays much higher overvoltages at the onset of the discharge plateau as the current rate increases. At 12.8 C where the failure is observed, the initial overvoltage exceeds the cut-off voltage ending the lithiation of the electrode prematurely. The LiPON protective layer appears to stabilize the electrode resulting in a flat discharge plateau even at 12.8 C. Further evidence for the resistive nature of the supposed SEI layer is revealed from electrochemical impedance spectroscopy (EIS) measurements. In the Nyquist plots (Figure 4d) an additional semicircle at mid-frequencies can be seen in the bare LiTP sample indicating increased cell resistance. Since the measurements were conducted in a two electrode setup, further deciphering of the EIS data was not attempted as it is not possible to separate the contributions of the LiTP working electrode and the Li-metal counter electrode.

The cycle life of the LiPON-coated LiTP electrode was investigated at current rates of 3.2 and 6.4 C (Figure 4e). At 3.2 C the electrode performance is exceptionally stable: 97.4 % of the initial capacity is retained even after 200 charge/discharge cycles. Accordingly, the coulombic efficiency is very high, 99.7 % on the average. As the current rate is increased to 6.4 C, a steady capacity fade can be observed. After 500 cycles the capacity remains at 81.8 % in respect to the 1st 6.4 C charge/discharge cycle while the coulombic efficiency remains high at 99.8 % on the average. From the voltage curves recorded at different stages of cycling, it could be confirmed that the

voltage profile remains stable throughout the cycling with no additional overpotentials associated with the aging of the electrodes (Figure S5a and S5b). Combined with the high coulombic efficiency, this seems to implicate that the capacity fade is mostly due to dissolution of the active material, which has previously been noted to be a contributing cause to the capacity fade of LiTP,[19] and not due to unwanted side reactions, e.g. formation of a resistive surface layer. Thus, while the intended application for the LiTP thin films is in all-solid-state LIBs, the current results may prove to be helpful also for bulk organic electrode materials highlighting the usefulness of a protective surface coating on the stability of the materials. Moreover, although more sophisticated analysis is needed, these results seem to implicate that also the LiTP-LiPON interface remains stable, which is crucial for the performance of an all-solid-state LIB.

In conclusion, we developed a simple reproducible ALD/MLD process for Li-containing inorganic-organic hybrid thin films. Our as-deposited Li terephthalate thin films were crystalline exhibiting the same layered crystal structure previously reported for bulk LiTP. Moreover demonstrated was that the films are electrochemically highly active showing excellent rate capabilities without any conductive additives. Most remarkably, a thin LiPON electrolyte coating applied using our recently reported ALD process was found to suppress the unwanted side reactions with the $LiPF_6$-based liquid electrolyte without increasing the cell resistance. Although further studies using an all-solid-state setup are required, the present findings appear to indicate that LiTP is a very promising candidate for a high-rate high-capacity anode material for thin-film LIBs. We believe that our work is a step towards the all-solid-state organic-electrode-based LIB technology, and has furthermore demonstrated the potential power of the ALD/MLD technique in realizing this technology.

Experimental Section

The LiTP thin films were deposited using an F-120 flow-type hot-wall ALD reactor (ASM Microchemistry Ltd.), from lithium 2,2,6,6-tetramethyl-3,5-heptanedionate (Li(thd)) and terephthalic acid (TPA). Li(thd) was synthesized in-house by mixing 50-% EtOH solutions of LiOH and Hthd. The resulting white precipitate was dried in vacuum and purified by sublimation. TPA (>99.0 %) was acquired from Tokyo Chemical Industry Co., Ltd. Both precursors were kept inside the reactor at temperatures of 175 °C for Li(thd) and 185 °C for TPA. Nitrogen (99.999%, produced from air by Schmidlin UHPN 3000 nitrogen generator) was used both as purging and carrier gas. The purging times were kept constant at 4 s for Li(thd) and 30 s for TPA. The films were deposited on Si(100) substrates for structural characterization and on stainless steel disks (15.5 mm diameter) for the electrochemical characterization. The reactor pressure was ~5 mbar. For the deposition of the LiPON coatings, lithium hexamethyldisilazide and diethyl phosphoramidate were used as the precursors.[24] The pulse/purge lengths were 2 s/2 s for both precursors with a total of 600 deposition cycles applied. The deposition temperature was 300 °C.

The thickness of the films was measured using a Semilab SE-2000 spectroscopic ellipsometer equipped with a xenon lamp. The crystallinity of the films was studied by grazing incidence X-ray diffraction using a PANanalytical X'Pert Pro diffractometer with a Cu K X-ray source while the density of the films was deduced from X-ray reflectivity measurements using the same device. The density of the films was calculated from the XRR patterns based on the dependency of the critical angle, θ_c, on the mean electron density, ρ_e, of the material; namely $\rho_e = (\theta_c^2\pi)/(\lambda^2 r_e)$, where λ is the X-ray wavelength and r_e is the classical electron radius. By assuming the elemental composition being that of pure LiTP, i.e. $Li_2C_8H_4O_4$, the mass density can be estimated from $\rho_m = (\rho_e A)/(N_A Z)$, where A is the average molar mass, N_A is the Avogadro constant and Z is the average atomic

number.[26] We note that the assumption on chemical composition and ambiguity in determining the exact critical angle result in uncertainties in the absolute value but still allows for extracting trends within a sample series. For samples up to 100 deposition cycles, XRR was also used to cross check the film thickness. The lattice constants were determined from the GIXRD pattern by Le Bail profile fitting procedure using the FullProf Software Suite.[27] The surface composition was analyzed with X-ray photoelectron spectroscopy (Kratos Analytical AXIS Ultra) with monochromatic Al-Kα radiation. The binding energy was calibrated based on C1s peak set to 285 eV. The FTIR measurements were conducted in a transmission mode on samples deposited on Si with a Nicolet Magna 750 spectrometer in range of 400-4000 cm^{-1} using a resolution of 4 cm^{-1}. The SEM images were collected on a JEOL JSM-7500FA scanning electron microscope. AFM measurements were conducted with a Veeco Dimension 5000 operated in tapping mode. For the electrochemical measurements, the films deposited on stainless steel substrates were dried in vacuum at 110 °C for 24 h and then used as the working electrode in a CR2016 coin cell. Lithium metal was used as the counter electrode and the electrolyte was 1 M $LiPF_6$ in 50:50 ethylene carbonate/dimethyl carbonate solution. The cell assembly was conducted in an Ar filled glove box with O_2 level less than 1 ppm and H_2O level less than 0.1 ppm. The cyclic voltammetry and electrochemical impedance spectroscopy measurements were carried out using an Autolab PGSTAT302N potentiostat/galvanostat. The EIS measurements were carried out in the frequency range of 500 kHz - 1 mHz using an amplitude of 10 mV. The galvanostatic measurements were conducted using a Neware battery testing unit.

ASSOCIATED CONTENT

Supporting information. SEM image of LiTP thin film deposited on microstructured Si-substrate, evolution of FWHM values of the 011 peak of LiTP from GIXRD as a function of film thickness, FTIR and XPS analysis on the aging of LiTP thin films, voltage profiles recorded during the cycling stability testing. This material is available free of charge via the Internet at http://pubs.acs.org.

AUTHOR INFORMATION

Corresponding Author

*maarit.karppinen@aalto.fi

Notes

The authors declare no competing financial interest.

Author Contributions

The manuscript was written through contributions of all authors. All authors have given approval to the final version of the manuscript.

ACKNOWLEDGEMENT

The present work has received funding from the European Research Council under the European Union's Seventh Framework Programme (FP/2007-2013)/ERC Advanced Grant Agreement (No. 339478). Dr. Erik Østreng is gratefully acknowledged for the ellipsometry measurements and discussions related to the growth mode. Dr. Leena-Sisko Johansson is thanked for carrying out the XPS measurements and Mr. Esko Ahvenniemi and Ms. Taina Rauhala for their assistance in the AFM and SEM measurements, respectively. This work made use of the Aalto Nanomicroscopy Center (Aalto NMC) facilities.

REFERENCES

1) Long, J. W.; Dunn, B.; Rolison, D. R.; White, H. S. *Chem. Rev.* **2004**, *104*, 4463–4492.

(2) Oudenhoven, J. F. M.; Baggetto, L.; Notten, P. H. L. *Adv. Energy Mater.* **2011**, *1*, 10–33.

(3) Roberts, M.; Johns, P.; Owen, J.; Brandell, D.; Edstrom, K.; El Enany, G.; Guery, C.; Golodnitsky, D.; Lacey, M.; Lecoeur, C.; Mazor, H.; Peled, E.; Perre, E.; Shaijumon, M. M.; Simon, P.; Taberna, P.-L. *J. Mater. Chem.* **2011**, *21*, 9876.

(4) Meng, X.; Yang, X.-Q.; Sun, X. *Adv. Mater.* **2012**, *24*, 3589–3615.

(5) Nilsen, O.; Miikkulainen, V.; Gandrud, K. B.; Østreng, E.; Ruud, A.; Fjellvåg, H. *Phys. Status Solidi* **2014**, *211*, 357–367.

(6) George, S. M. *Chem. Rev.* **2010**, *110*, 111–131.

(7) Liang, Y.; Tao, Z.; Chen, J. *Adv. Energy Mater.* **2012**, *2*, 742–769.

(8) Häupler, B.; Wild, A.; Schubert, U. S. *Adv. Energy Mater.* **2015**, *5*, 14020434.

(9) Sundberg, P.; Karppinen, M. *Beilstein J. Nanotechnol.* **2014**, *5*, 1104–1136.

(10) Armand, M.; Grugeon, S.; Vezin, H.; Laruelle, S.; Ribière, P.; Poizot, P.; Tarascon, J.-M. *Nature Mater.* **2009**, *8*, 120–125.

(11) Zhang, Y. Y.; Sun, Y. Y.; Du, S. X.; Gao, H. J.; Zhang, S. B. *Appl. Phys. Lett.* **2012**, *100*, 091905.

(12) Patil, A.; Patil, V.; Wook Shin, D.; Choi, J. W.; Paik, D. S.; Yoon, S. J. *Mater. Res. Bull.* **2008**, *43*, 1913–1942.

(13) Sundberg, P.; Karppinen, M. *Eur. J. Inorg. Chem.* **2014**, 968–974.

(14) Lee, B. H.; Yoon, B.; Abdulagatov, A. I.; Hall, R. A.; George, S. M. *Adv. Funct. Mater.* **2013**, *23*, 532–546.

(15) Nilsen, O.; Karlsen, O. B.; Kjekshus, A.; Fjellvåg, H. *Thin Solid Films* **2007**, *515*, 4550–4558.

(16) Nilsen, O.; Mohn, C. E.; Kjekshus, A.; Fjellvåg, H. *J. Appl. Phys.* **2007**, *102*, 024906.

(17) Ahvenniemi, E.; Karppinen, M. *Chem. Commun.* **2015**, *52*, 1139–1142.

(18) Kaduk, J. *Acta Crystallogr. Sect. B Struct. Sci.* **2000**, *56*, 474–485.

(19) Yu, Q.; Chen, D.; Liang, J.; Chu, Y.; Wu, Y.; Zhang, W.; Li, Y.; Li, L.; Zeng, R. *RSC Adv.* **2014**, *4*, 59498–59502.

(20) Verpoort, F.; Haemers, T.; Roose, P.; Maes, J. P. *Appl. Spectrosc.* **1999**, *53*, 1528–1534.

(21) Klepper, K. B.; Nilsen, O.; Fjellvåg, H. *Dalton Trans.* **2010**, *39*, 11628–11635.

(22) Téllez S., C. A.; Hollauer, E.; Mondragon, M. A.; Castaño, V. M. *Spectrochim. Acta - Part A Mol. Biomol. Spectrosc.* **2001**, *57*, 993–1007.

(23) Schroder, K. W.; Celio, H.; Webb, L. J.; Stevenson, K. J. *J. Phys. Chem. C* **2012**, *116*, 19737–19747.

(24) Nisula, M.; Shindo, Y.; Koga, H.; Karppinen, M. *Chem. Mater.* **2015**, *27*, 6987–6993.

(25) Lee, H. H.; Park, Y.; Shin, K.; Lee, K. T.; Hong, S. Y. *ACS Appl. Mater. Interfaces* **2014**, *6*, 19118–19126.

(26) Holy, V.; Pietsch, U.; Baumbach, T. *High Resolution X-Ray Scattering from Thin Films and Multilayers*, Springer-Verlag, Berlin, 1999, p. 127.

(27) Rodríguez-Carvajal, J. *Phys. B Condens. Matter* **1993**, *192*, 55–69.

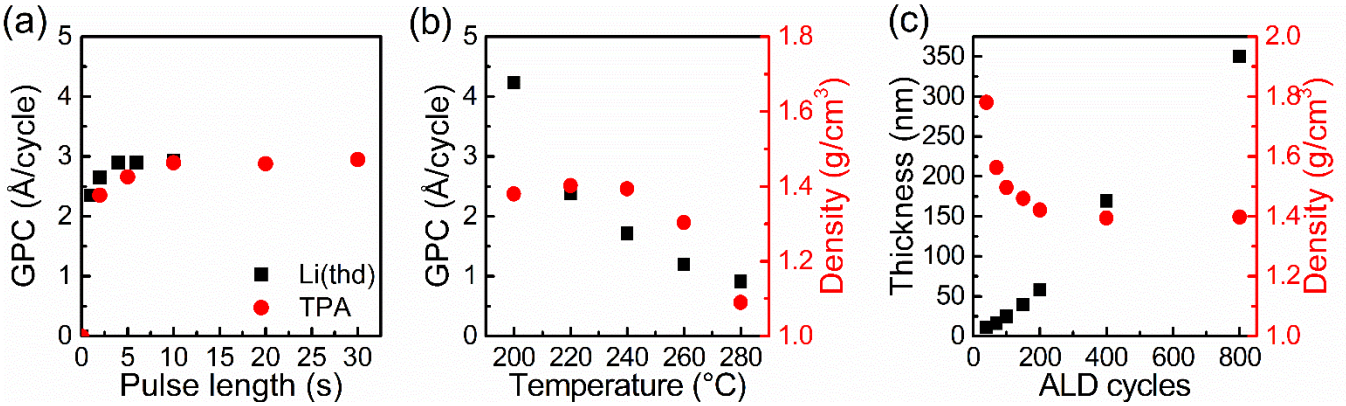

Figure 1. (a) Growth-per-cycle (GPC) of LiTP thin films as a function of Li(thd) (black squares) and TPA (red circles) pulse lengths. The deposition temperature was 200 °C and the pulse/purge lengths of the other precursor were fixed to 4 s/4 s for Li(thd) and to 10 s/30 s for TPA. (b) GPC (black squares) and film density (red circles) of LiTP as a function of deposition temperature. The pulse/purge lengths were 4 s/4 s and 10 s/30 s for Li(thd) and TPA, respectively. (c) Film thickness (black squares) and density (red circles) of LiTP versus number of deposition cycles. The deposition temperature was 200 °C and the pulse/purge lengths were 4 s/4 s and 10 s/30 s for Li(thd) and TPA, respectively.

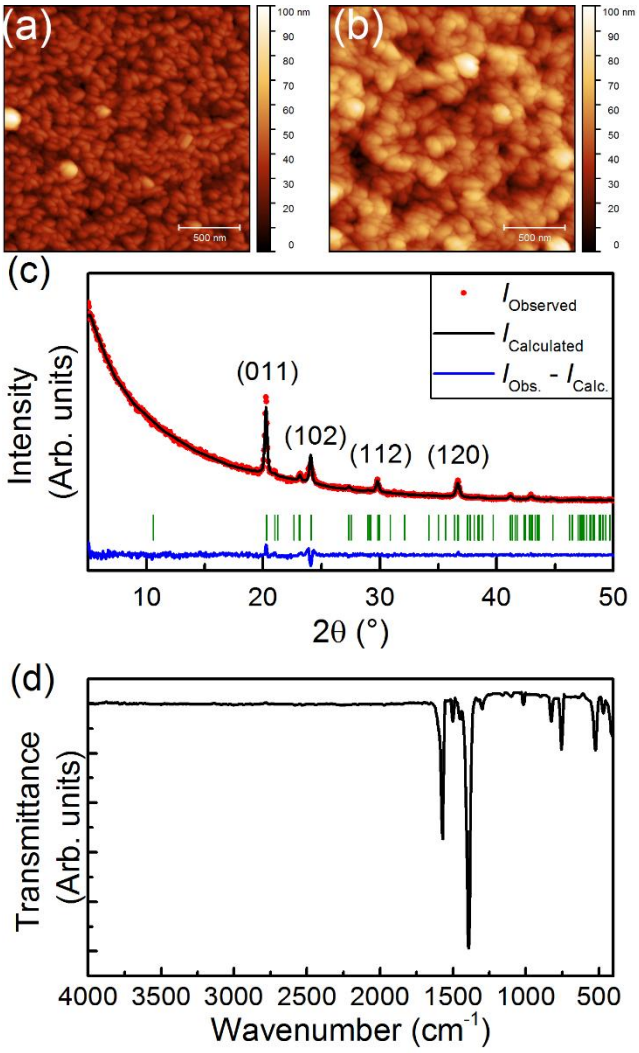

379

380 **Figure 2.** AFM images of samples with (a) 70 and (b) 400 deposition cycles, (c) GIXRD pattern

381 for a LiTP film deposited at 200 °C using 400 deposition cycles. (d) FTIR spectrum of the same

382 film.

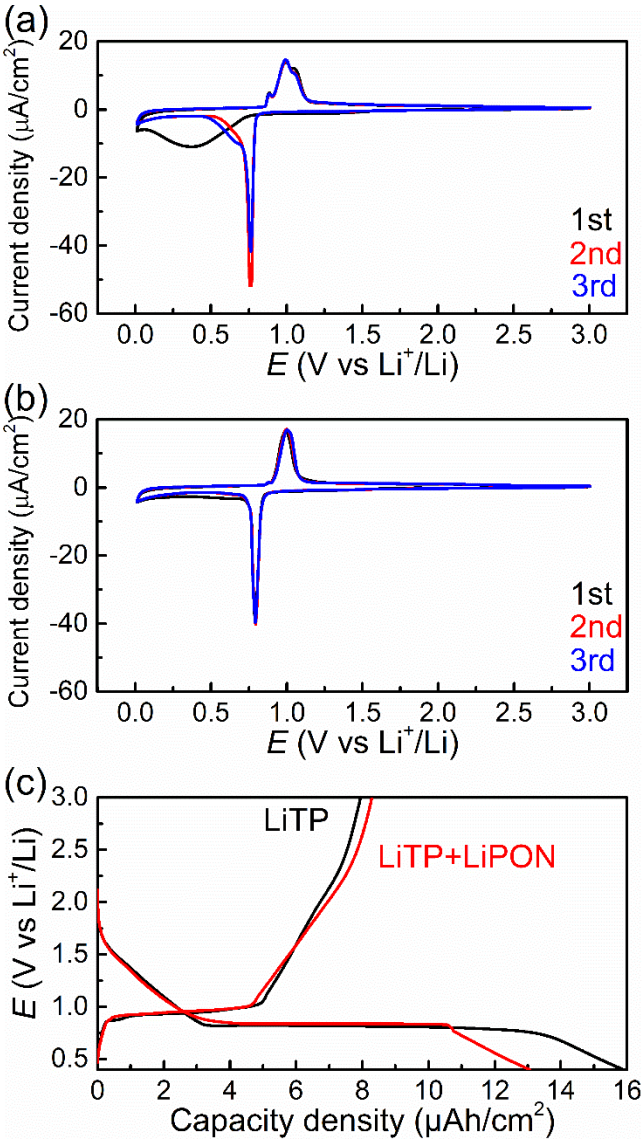

383

384 **Figure 3.** Cyclic voltammograms of (a) bare, and (b) LiPON-coated LiTP conducted at a scan rate

385 of 0.1 mV/s. (c) The initial charge/discharge curves of LiTP (black line) and LiTP-LiPON (red

386 line) recorded using a current density of 0.5 μA/cm^2 (~0.05 C).

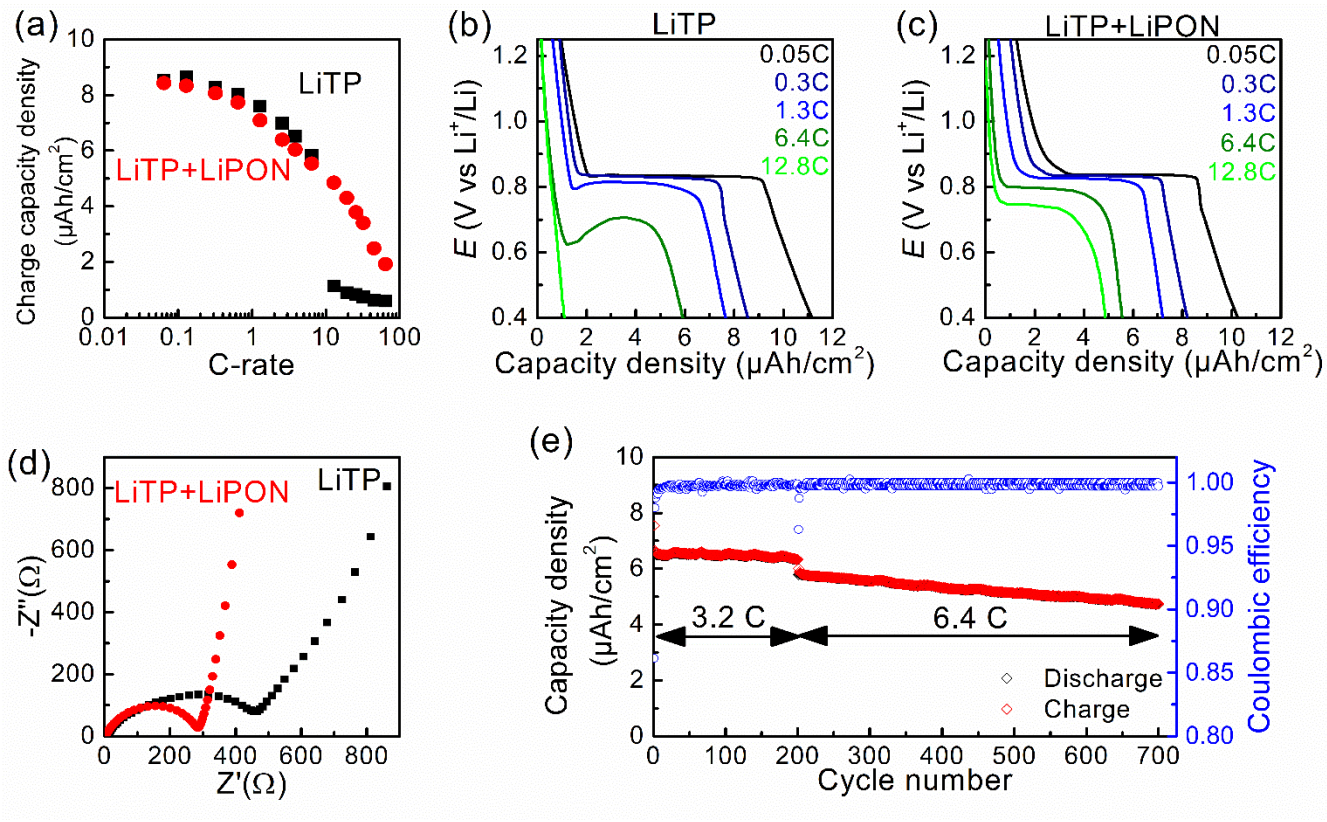

387

388 **Figure 4.** (a) Rate capability of bare LiTP (black squares) and LiPON-coated LiTP (red circles) as
389 determined from the charge capacity. Discharge curves at different current rates for (b) LiTP, and
390 (c) LiPON-coated LiTP. In the bare LiTP at 12.8 C the overvoltage exceeds the cut-off potential
391 ending the lithiation prematurely. (d) Nyqvist plots of the EIS measurements for LiTP (black
392 squares) and LiPON-coated LiTP (red circles). (e) Cycle life of LiPON-coated LiTP measured at
393 current rates of 3.2 and 6.4 C.

394

395 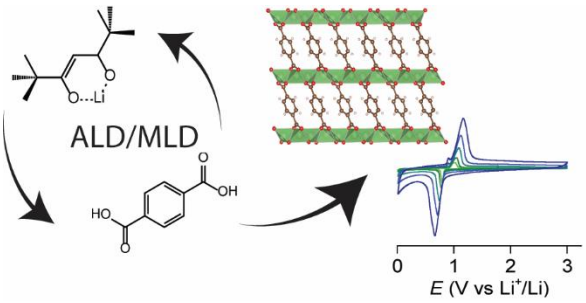

396 For table of contents only